1392 *Chem. Mater.* **2010,** *22,* 1392–1401
DOI:10.1021/cm902876u

CHEMISTRY OF MATERIALS
Article

Graphene/Polyaniline Nanofiber Composites as Supercapacitor Electrodes

Kai Zhang,[†] Li Li Zhang,[‡] X. S. Zhao,*[,‡] and Jishan Wu*[,†]

[†]*Department of Chemistry, National University of Singapore, 3 Science Drive 3, 117543, Singapore, and* [‡]*Department of Chemical and Biomolecular Engineering, National University of Singapore, 4 Engineering Drive 4, Singapore 117576, Singapore*

Received September 15, 2009. Revised Manuscript Received December 18, 2009

Chemically modified graphene and polyaniline (PANI) nanofiber composites were prepared by in situ polymerization of aniline monomer in the presence of graphene oxide under acid conditions. The obtained graphene oxide/PANI composites with different mass ratios were reduced to graphene using hydrazine followed by reoxidation and reprotonation of the reduced PANI to give the graphene/PANI nanocomposites. The morphology, composition, and electronic structure of the composites together with pure polyaniline fibers (**PANI-F**), graphene oxide (**GO**), and graphene (**GR**) were characterized using X-ray diffraction (XRD), solid-state ^{13}C NMR, FT-IR, scanning electron microscope (SEM), transmission electron microscope (TEM), thermogravimetric analysis (TGA), and X-ray photoelectron spectroscopy (XPS). It was found that the chemically modified graphene and the PANI nanofibers formed a uniform nanocomposite with the PANI fibers absorbed on the graphene surface and/or filled between the graphene sheets. Such uniform structure together with the observed high conductivities afforded high specific capacitance and good cycling stability during the charge−discharge process when used as supercapacitor electrodes. A specific capacitance of as high as 480 F/g at a current density of 0.1 A/g was achieved over a PANI-doped graphene composite. The research data revealed that high specific capacitance and good cycling stability can be achieved either by doping chemically modified graphenes with PANI or by doping the bulky PANIs with graphene/graphene oxide.

1. Introduction

In the wake of increasing pollution and depleting of traditional energy resource, the development of renewable energy production and hybrid electric vehicles with low CO_2 emission have been attracting much attention since the end of last century.[1] Meanwhile, great efforts have gone into developing lithium ion and other secondary batteries to store energy for autonomy purpose.[2] However, with the growing demand for portable systems and hybrid electric vehicles, which require high power in short-term pulses, the electrochemical capacitors are gathering pace.[3] Compared with secondary batteries, electrochemical capacitors, also known as supercapacitors or ultracapacitors, exhibit faster and higher power capability, long life, wide thermal operating range, and low maintenance cost.[4]

Supercapacitors have two energy storage mechanisms, namely the electrical double-layer (EDL) capacitance and the pseudocapacitance.[3a] For EDL capacitors, carbon-based materials with a high surface area are usually used, and the capacitance comes from the charge accumulated at the electrode/electrolyte interface.[5] On the other hand, the pseudocapacitors or redox supercapacitors use conducting polymers and metal oxides as electrode materials, which undergo fast and reversible faradic redox reaction.[6] Among various materials used for supercapacitors, lightweight conducting polymers such as polyanilines (PANIs),[7] polypyrroles (PPYs),[8] and polythiophenes (PTs)[9] have been shown to display high capacitances.

*Corresponding author e-mail: chmwuj@nus.edu.sg; chezxs@nus.edu.sg.

(1) Simon, P.; Gogotsi, Y. *Nat. Mater.* **2008**, *7*, 845–854.
(2) (a) Tarascon, J. M.; Armand, M. *Nature* **2001**, *414*, 359–367. (b) Arico, A. S.; Bruce, P.; Scrosati, B.; Tarascon, J. M.; Van Schalkwijk, W. *Nat. Mater.* **2005**, *4*, 366–377.
(3) (a) Conway, B. E. *Electrochemical Supercapacitors: Scientific Fundamentals and Technological Applications*; Kluwer: **1999**. (b) Miller, J. R.; Simon, P. *Science* **2008**, *321*, 651–652.
(4) (a) Winter, M.; Brodd, R. J. *Chem. Rev.* **2004**, *104*, 4245–4269. (b) Pandolfo, A. G.; Hollenkamp, A. F. *J. Power Sources* **2006**, *157*, 11–27.
(5) Nishino, A. *Proc. Electrochem. Soc.* **1993**, *93*−*23*, 1.
(6) Conway, B. E. *Proc. Electrochem. Soc.* **1995**, *93*−*29*, 15.
(7) (a) Jang, J. *Adv. Polym. Sci.* **2006**, *199*, 189–259. (b) Fusalba, F.; Gouerec., P.; Belanger, D. *J. Electrochem. Soc.* **2001**, *148*, A1. (c) Hu, C. C.; Chu, C. H. *Mater. Chem. Phys.* **2000**, *65*, 329–338. (d) Ryu, K. S.; Kim, K. M.; Park, N.-G.; Park, Y. J.; Chang, S. H. *J. Power Sources* **2002**, *103*, 305–309. (e) Gupta, V.; Miura, N. *Electrochem. Solid-State Lett.* **2005**, *8*, A630–632. (f) Bélanger, D.; Ren, X.; Davey, J.; Uribe, F.; Gottesfeld, S. *J. Electrochem. Soc.* **2000**, *147*, 2923–2929.
(8) (a) Frackowiak, E.; Khomenko, V.; Jurewicz, K.; Lota, K.; Béguin, F. *J. Power Sources* **2006**, *153*, 413–418. (b) Jurewicz, K.; Delpeux, S.; Bertaggna, V.; Béguin, F.; Frackowiak, E. *Chem. Phys. Lett.* **2001**, *347*, 36–40.
(9) (a) Rudge, A.; Davey, J.; Raistrick, I.; Gottesfeld, S.; Ferraris, J. P. *J. Power Sources* **1994**, *47*, 89–107. (b) Laforgue, A.; Simon, P.; Sarrazin, C.; Fauvarque, J.-F. *J. Power Sources* **1999**, *80*, 142–148. (c) Mastragostino, M.; Arbizzani, C.; Soavi, F. *J. Power Sources* **2001**, *97*−*98*, 812–815. (d) Arbizzani, C.; Mastragostino, M.; Soavi, F. *J. Power Sources* **2001**, *100*, 164–170.

 Published on Web 01/27/2010

However, they also exhibit poor stabilities during the charge/discharge process. Carbon materials such as activated carbon (AC), mesoporous carbon (MC), and carbon nanotubes (CNTs) usually display good stability, but the capacitance values are limited by the microstructures in the materials.[10] Therefore, composite materials based on CNTs and conducting polymers such as PANIs have been tested as supercapacitor electrodes and high capacitances and improved stability have been achieved[11] due to the synergetic combination of the excellent conducting and mechanical properties of CNTs and high pseudocapacitance of the PANIs. However, pristine CNTs are very expensive and mainly possess electric double-layer capacitance only up to 80 F/g.[12]

Recently, graphene, a two-dimensional all-sp^2-hybridized carbon with unique electronic and mechanical properties, has received a rapidly growing research interest.[13] Graphene and chemically modified graphene sheets possess high conductivity,[14] high surface area, and good mechanical properties[15] comparable with or even better than CNTs. In addition, graphene-based materials can be easily obtained by simple chemical processing of graphite.[16] Therefore, the potential of using graphene-based materials for supercapacitor has attracted much attention very recently.[17] In fact, specific capacitances of tens to 135 F/g have been determined for different graphene materials.[17a] The observed capacitances are mainly limited by the agglomeration of graphene sheets and do not reflect the intrinsic capacitance of an individual graphene sheet. Very recently, an experimental determination of EDL capacitance ($\sim$21 μFcm^{-2}) and quantum capacitance of single layer and double-layer graphene was reported.[17b]

To exploit the potential of graphene-based materials for supercapacitor applications, graphene/polyaniline composite paper was prepared by in situ anodic electropolymerization of aniline on graphene paper, and electrochemical capacitance as high as 233 F/g was achieved.[18] However, the capacitance was mainly dominated by the pseudocapacitance from the polyaniline films coated on the graphene paper surface, and the electric double layer capacitance from the graphene sheet was less utilized due to the agglomerated layerlike structure in the graphene paper. Meanwhile, graphene oxide (GO) and graphene nanosheets have also been doped into polyaniline matrix.[19] In the former case, only a small amount of insulating GO (e.g., 1%) was used because excess GO will reduce the conductivity of the composite.[19a] In the later cases, graphene nanosheets were first prepared by reduction of graphene oxide followed with polymerization of aniline, and the graphene sheets were also in a partially agglomerated form.[19b,c] Here we demonstrate the preparation of graphene/PANI composites using an in situ polymerization method, aimed to achieve a *homogeneous* dispersion of individual graphene sheets within the polymer matrix. The aniline monomer was first mixed with graphene oxide sheets in aqueous solution by sonicating to form a homogeneous suspension. Then, oxidant was added to this mixture to obtain the homogeneous composites of graphene oxide sheets/PANI nanofibers. Finally, the composites were reduced by hydrazine and followed with reoxidation and reprotonation to give the composites of graphene sheets/PANI nanofibers. The mass ratio of graphene over PANI was tuned to make the composites either with polyaniline as the main component (i.e., graphene-doped PANIs) or with the graphene sheets as the main component (i.e., PANI-doped graphenes). Previous research has also shown that fibrous PANIs with large surface area usually show larger capacitance than the normal PANI particles.[7e,20] Thus in this work, the PANIs in the composites were controlled in the fibrous forms. The obtained composite materials with different compositions showed very good electrochemical performances.

2. Experimental Section

Preparation of Graphene Oxide (GO). Graphene oxide was synthesized from natural graphite (crystalline, 300 mesh, Alfa Aesar) by a modified Hummers method.[21] Graphite (5 g) and $NaNO_3$ (2.5 g) were mixed with 120 mL of H_2SO_4 (95%) in a 500 mL flask. The mixture was stirred for 30 min within an ice bath. While maintaining vigorous stirring, potassium permanganate

(10) (a) Futaba, D. N.; Hata, K.; Yamada, T.; Hiraoka, T.; Hayamizu, Y.; Kakudate, Y.; Tanaike, O.; Hatori, H.; Yumura, M.; Iijima, S. *Nat. Mater.* **2006**, *5*, 987–994. (b) Portet, C.; Chmiola, J.; Gogotsi, Y.; Park, S.; Lian, K. *Electrochim. Acta* **2008**, *53*, 7675–7680. (c) Yang, C. M.; Kim, Y. J.; Endo, M.; Kanoh, H.; Yudasaka, M.; Iijima, S.; Kaneko, K. *J. Am. Chem. Soc.* **2007**, *129*, 20–21. (d) Zhang, L. L.; Zhao, X. S. *Chem. Soc. Rev.* **2009**, *38*, 2520–2531.

(11) (a) Kong, L. B.; Zhang, J.; An, J. J.; Luo, Y. C.; Kang, L. *J. Mater. Sci.* **2008**, *43*, 3664–3669. (b) Sivakkumar, S. R.; Kim, W. J.; Choi, J. A.; MacFarlane, D. R.; Forsyth, M.; Kim, D. W. *J. Power Sources* **2007**, *171*, 1062–1068. (c) Mi, H. Y.; Zhang, X. G.; An, S. Y.; Ye, X. G.; Yang, S. D. *Electrochem. Commun.* **2007**, *9*, 2859–2862. (d) Frackowiak, E.; Khomenko, V.; Jurewicz, K.; Lota, K.; Béguim, F. *J. Power Sources* **2006**, *153*, 413–418.

(12) Niu, C.; Sichel, E. K.; Hoch, R.; Moy, D.; Tennent, H. *Appl. Phys. Lett.* **1997**, *70*, 1480–1483.

(13) (a) Geim, A. K.; Novoselov, K. S. Nat. Mater. **2007**, *6*, 183−191, and references therein. (b) Wu, J. S.; Pisula, W.; Müllen, K. *Chem. Rev.* **2007**, *107*, 718–747. (c) Bunch, J. S.; van der Zande, A. M.; Verbridge, S. S.; Frank, I. W.; Tanenbaum, D. M.; Parpia, J. M.; Craighead, H. G.; McEuen, P. L. *Science* **2007**, *315*, 490–493. (d) Dikin, D. A.; Stankovich, S.; Zimney, E. J.; Piner, R. D.; Dommett, G. H. B.; Evmnenko, G.; Nguyen, S. T.; Ruoff, R. S. *Nature* **2007**, *448*, 457–460. (e) Wang, X.; Zhi, L. J.; Müllen, K. *Nano Lett.* **2008**, *8*, 323–327.

(14) Gomez-Navarro, C.; Weitz, R. T.; Bittner, A. M.; Scolari, M.; Mews, A.; Burghard, M.; Kern, K. *Nano Lett.* **2007**, *7*, 3499–3503.

(15) Stankovich, S.; Dikin, D. A.; Dommett, G. H. B.; Kohlhaas, K. M.; Zimney, E. J.; Stach, E. A.; Piner, R. D.; Nguyen, S. T.; Ruoff, R. S. *Nature* **2006**, *442*, 282–286.

(16) Ruoff, R. Nat. Nanotechnol. **2008**, *3*, 10−11, and references therein.

(17) (a) Stoller, M. D.; Park, S.; Zhu, Y.; An, J.; Ruoff, R. S. *Nano Lett.* **2008**, *8*, 3498–3502. (b) Xia, J. L.; Chen, F.; Li, J. H.; Tao, N. J. *Nat. Nanotechnol.* **2009**, *4*, 505–509. (c) Vivekchand, S. R. C.; Rout, C. S.; Subrahmanyam, K. S.; Govindara, A.; Rao, C. N. R. *J. Chem. Sci.* **2008**, *120*, 9–13.

(18) Wang, D. W.; Li, F.; Zhao, J.; Ren, W.; Chen, Z.-G.; Tan, J.; Wu, Z.-S.; Gentle, I.; Li, G. Q.; Cheng, H.-M. *ACS Nano* **2009**, *3*, 1745–1752.

(19) (a) Wang, H.; Hao, Q.; Yang, X.; Lu, L.; Wang, X. *Electrochem. Commun.* **2009**, *11*, 1158–1161. (b) Yan, J.; Wei, T.; Shao, B.; Fan, Z.; Qian, W.; Zhang, M.; Wei, F. *Carbon* **2010**, *48*, 487–493. (c) Vadivel Murugan, A.; Muraliganth, T.; Manthiram, A. *Chem. Mater.* **2009**, *21*, 5004–5006.

(20) Ganesan, R.; Shanmugam, S.; Gedanken, A. *Synth. Met.* **2008**, *158*, 848–853.

(21) (a) Becerril, H. A.; Mao, J.; Liu, Z.; Stoltenberg, R. M.; Bao, Z.; Chen, Y. *ACS Nano* **2008**, *2*, 463–470. (b) Hummers, W. S., Jr.; Offeman, R. E. *J. Am. Chem. Soc.* **1958**, *80*, 1339.

(15 g) was added to the suspension. The rate of addition was carefully controlled to keep the reaction temperature lower than 20 °C. The ice bath was then removed, and the mixture was stirred at room temperature overnight. As the reaction progressed, the mixture gradually became pasty, and the color turned into light brownish. At the end, 150 mL of H_2O was slowly added to the pasty with vigorous agitation. The reaction temperature was rapidly increased to 98 °C with effervescence, and the color changed to yellow. The diluted suspension was stirred at 98 °C for one day. Then, 50 mL of 30% H_2O_2 was added to the mixture. For purification, the mixture was washed by rinsing and centrifugation with 5% HCl and then deionized (DI) water for several times. After filtration and dry under vacuum, the graphene oxide (**GO**) was obtained as a gray powder.

Reduction of Graphene Oxide. Chemical conversion of graphene oxide to reduced graphene oxide (**GR**) was done according to the reported method.[22] In a typical experiment, 0.1 g of graphene oxide was dispersed in 50 mL of DI water. Then 0.1 mL of hydrazine monohydrate was added, and the mixture was heated at 95 °C for 1 h. Once the reaction is completed, the reduced graphene oxide (**GR**) was collected by filtration as a black powder. The obtained cake was washed with DI water several times to remove the excess hydrazine, and the final product was dried in a vacuum oven at 80 °C.

Preparation of Polyaniline Nanofibers (PANI-F). Polyaniline nanofibers were synthesized by a rapid mixing reaction.[23] Aniline was first distilled under vacuum to remove the oxidation impurities. The purified aniline (0.3 g, 3.2 mmol) was dissolved in 10 mL of 1 M HCl aqueous solution. While maintaining vigorous stirring at room temperature, ammonium peroxydisulfate (0.18 g, 0.8 mmol) in 10 mL of 1 M HCl aqueous solution was rapidly poured into the aniline solution. Polymerization was observed in about 5 min when the characteristic green color of polyaniline emeraldine salt appeared. The mixture was allowed to stir at room temperature overnight. At the end, the mixture was diluted by 100 mL of water. The precipitated polymer was collected by filtration and repetitively washed with water, ethanol, and hexane until the filtrate became colorless. After having been dried under vacuum at 60 °C, the **PANI-F** sample (0.08 g) was collected as a deep blue powder in 27% yield.

Preparation of Polyaniline-Graphene Oxide Composites. Homogenous composites of graphene oxide and polyaniline nanofibers were prepared by in situ polymerization of aniline in a suspension of graphene oxide in acidic solution. The weight feed ratio of aniline to graphene oxide was varied as 90:10, 50:50, and 20:80, and the resulting composites were named as **PAGO10**, **PAGO50**, and **PAGO80**, respectively. Typically, the purified aniline was dissolved in 1 M HCl at a concentration of 0.3 M. Graphene oxide was dispersed in the resulting solution by bath-sonicating for 1 h. While maintaining vigorous stirring at room temperature, another solution of ammonium peroxydisulfate, with a mole ratio to aniline of 1:4, in 1 M HCl was rapidly poured to the mixture. Polymerization of aniline started after about 5 min, while the color of the mixture changed into green. The mixture was allowed to stir at room temperature overnight and then diluted by 100 mL of water. The composites were collected by filtration and repetitively washed with water, ethanol, and hexane until the filtrate become colorless. The real mass percentages of the polyaniline in the composites are estimated as 73% for **PAGO10**, 20% for **PAGO50**, and 5% for **PAGO80** by weighting the **GO** powder before and after polymerization.

Scheme 1. Illustration of the Process for Preparation of Graphene-PANI Composites

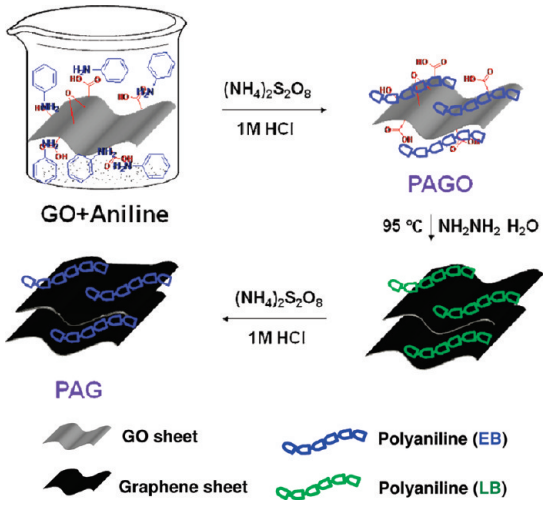

Preparation of the Graphene-Polyaniline Nanofiber Composites. The polyaniline-graphene oxide composites (**PAGO10**, **PAGO50**, and **PAGO80**) were reduced by hydrazine following a similar procedure to that for **GR**. Typically, 0.1 g of composite was heated with 0.1 mL of hydrazine in 50 mL of water at 95 °C for 1 h. The reduced composite was filtered and repetitively washed with DI water to remove excess hydrazine. The resulting material was dispersed in 10 mL of 1 M HCl solution containing 0.06 g of ammonium peroxydisulfate. The mixture was stirred at room temperature overnight, and the powder was collected by filtration and repetitively washed with DI water, ethanol, and hexane. The final composites were dried at 60 °C in a vacuum oven, and the dry powder was named as **PAG10**, **PAG50**, and **PAG80**, respectively.

General Characterization. Transmission electron microscope (TEM) measurements were conducted on A JEOL 2010 FEG microscope at 200 keV. The TEM samples were prepared by dispensing a small amount of dry powder in ethanol. Then, one drop of the suspension was dropped on 300 mesh copper TEM grids covered with thin amorphous carbon films. Scanning electron microscope (SEM) measurements were carried out a field emission scanning electron microanalyzer (JEOL-6300F) at 5 kV. The SEM sample was prepared by placing a drop of dilute ethanol dispersion of the composites onto a copper plate attached to an aluminum sample holder, and the solvent was allowed to evaporate at room temperature. X-ray diffraction (XRD) patterns of the composites were measured on a Bruker-AXS D8 DISCOVER with GADDS Powder X-ray diffractometer. Copper K_α line was used as a radiation source with λ = 1.5406 Å. X-ray photoelectron spectroscopy (XPS) analysis was carried out on an AXIS HIS 165 spectrometer (Kratos Analytical) using a monochromatized Al Kα X-ray source (1486.71 eV photons). Infrared spectra were recorded on a Varian 3100 FT-IR spectrometer by using pressed KBr pellets. High-resolution solid-state ^{13}C NMR experiments were carried out on a Bruker DRX-400 MHz NMR spectrometer. Thermogravimetric analysis (TGA) was carried out on a TA Instruments

(22) Stankovich, S.; Dikin, D. A.; Piner, R. D.; Kohlhaas, K. A.; Kleinhammes, A.; Jia, Y.; Wu, Y.; Nguyen, S. T.; Ruoff, R. S. *Carbon* **2007**, *45*, 1558–1565.
(23) (a) Huang, J.; Kaner, R. B. *Angew. Chem., Int. Ed.* **2004**, *43*, 5817–5821. (b) Huang, J.; Virji, S.; Weiller, B. H.; Kaner, R. B. *J. Am. Chem. Soc.* **2003**, *125*, 314–315. (c) Huang, J. X. *Pure Appl. Chem.* **2006**, *78*, 15–27. (d) Li, D.; Huang, J. X.; Kaner, R. B. *Acc. Chem. Res.* **2009**, *42*, 135–145.

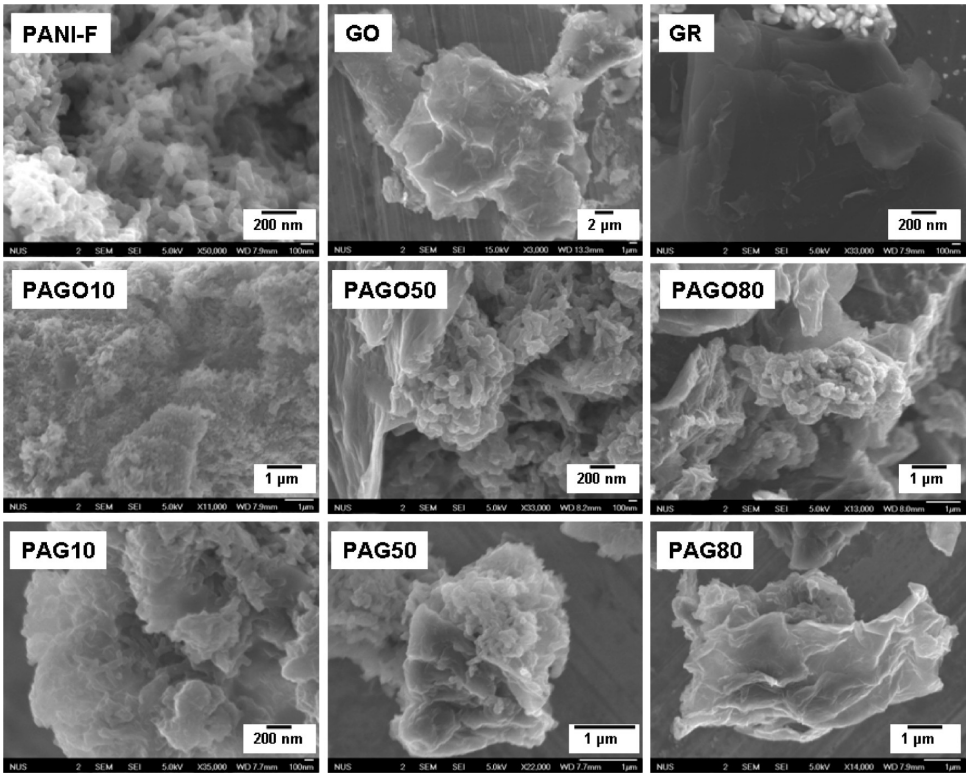

Figure 1. Representative SEM images of **PANI-F**, **GO**, **GR**, **PAGO10**, **PAGO50**, **PAGO80**, **PAG10**, **PAG50**, and **PAG80**.

2960 at a heating rate of 10 °C/min under nitrogen flow. The Bulk DC conductivity measurements of the composites were made on pressed pellets (1.3 cm diameter, <1 mm thickness) with an Alessi four-probe-point conductivity probe. A Keithley 617 programmable electrometer and a Keithley 224 programmable current source were used for the measurement of voltage as a function of current. The specific surface areas (S_{BET}) were determined according to the Brunauer−Emmett−Teller (BET) plot of nitrogen adsorption isotherm in the relative pressure range of 0.05−0.2.

Electrochemical Measurements. The working electrode was prepared by casting a nafion-impregnated sample onto a glassy carbon electrode with a diameter of 5 mm. Typically, 5 mg of a composite was dispersed in 1 mL of an ethanol solution containing 5 μL of a nafion solution (5 wt % in water) by sonication for 20 min. This sample was then dropped onto the glassy carbon electrode and dried in an oven before the electrochemical test. A three-electrode cell system was used to evaluate the electrochemical performance by electrochemical impedance spectroscopy, cyclic voltammetry (CV), and galvanostatic charge−discharge techniques on an Autolab PGSTAT302N at room temperature. The electrolyte used is a 2 M H_2SO_4 aqueous solution. A platinum sheet and a AgCl/Ag electrode were used as the counter and the reference electrodes, respectively.

3. Results and Discussion

3.1. Preparation of Graphene/Polyaniline Nanofiber Composites. The preparation method is illustrated in Scheme 1. First, the graphene oxide (**GO**) was prepared according to a modified Hummer's method.[21] It is known that **GO** can form stable suspension in water, and, thus, a homogeneous mixture of **GO** in acidic solution (1 M HCl) containing various amounts of aniline can be easily obtained. Under vigorous stirring, oxidant ammonium peroxydisulfate (APS) in 1 M HCl solution was rapidly added, and the mixture was stirred at room temperature overnight to generate a polyaniline-graphene oxide composite. Based on the mass feed ratios of the aniline monomer to the graphene oxide (10%, 50%, and 80% **GO**), the obtained composites are designed as **PAGO10**, **PAGO50**, and **PAGO80**, respectively. Under such fast mixing conditions, polyaniline fibers are believed to form in the composites.[23] In situ polymerization of aniline in the presence of **GO** in the acidic aqueous solution allowed us to prepare homogeneous composites in which PANI and **GO** are believed to intercalate with each other instead of individually being in an agglomerated form as observed previously.[17a,c] The composites were then treated with hydrazine at 95 °C for 1 h. Most **GO** is believed to have been reduced to form conductive graphene sheets.[22] However, the PANI in the composites may have also been reduced from the highly conductive halfly oxidized emeraldine base (EB) state to the reduced, neutral leucoemeraldine (LB) state during the reduction process,[24] so reoxidation and reprotonation are necessary to recover the conductive PANI structure after the reduction of GO. The reduced composites were then stirred in 1 M HCl solution in the presence of ammonium peroxydisulfate at room temperature overnight. After filtration, washing, and drying, polyaniline/graphene composites, designed as **PAG10**, **PAG50**, and **PAG80**, respectively, were obtained from the corresponding polyaniline/GO composites.

(24) (a) Wang, L. X.; Jing, X. B.; Wang, F. S. *Synth. Met.* **1991**, *41−43*, 739–744. (b) Fukuda, T.; Takezoe, H.; Ishikawa, K.; Fukuda, A.; Woo, H. S.; Jeong, S. K.; Oh, E. J.; Suh, J. S. *Synth. Met.* **1995**, *69*, 175–176. (c) Zeng, X. R.; Ko, T. M. *Polymer* **1998**, *39*, 1187–1195.

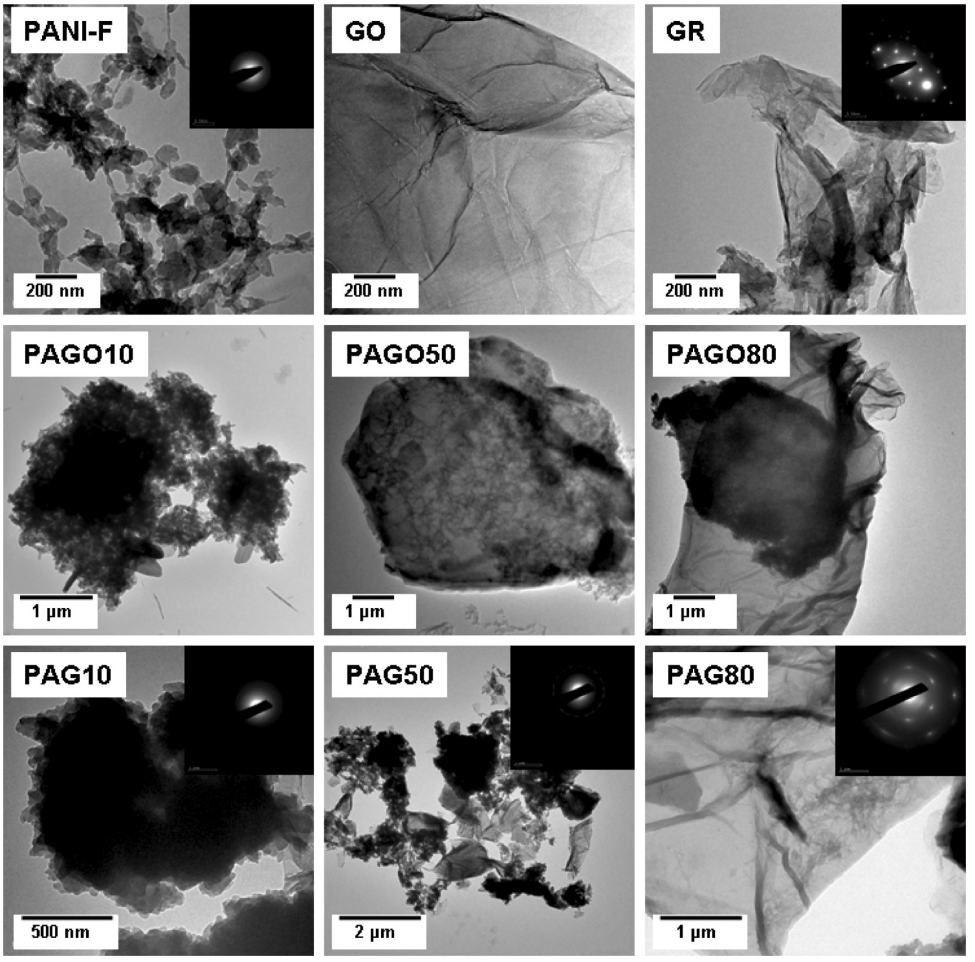

Figure 2. Representative TEM images of **PANI-F**, **GO**, **GR**, **PAGO10**, **PAGO50**, **PAGO80**, **PAG10**, **PAG50**, and **PAG80**. Inserts are the selected area electron diffraction patterns of some composites.

For comparison purposes, pure polyaniline nanofibers (**PANI-F**) and reduced graphene (**GR**) were also prepared via the similar polymerization and reduction processes as described above.

3.2. Morphology and Structure. The morphology and structure of the **PANI-F**, **GO**, **GR** and all composites were characterized using scanning electron microscope (SEM) and transmission electron microscope (TEM). The results are shown in Figures 1 and 2, respectively. The pure polyaniline prepared by the rapid mixing method shows uniform fibrous structures of hundreds of nanometers in length and about 50 nm in width. The selected area electron diffraction (SAED) patterns from these PANI fibers disclose that the **PANI-F** materials are a lack of obvious crystalline character (Figure 2). The **GO** prepared here has a typically curved, layerlike structure with the size of tens of micrometers. The reduced form **GR** however mainly agglomerated into graphene-like particles with the sheets structure having good crystalline character as shown by the SAED pattern (Figure 2).

For composites **PAGO10** and **PAGO50**, SEM and TEM images show that all the graphene oxide sheets are homogeneously surrounded with PANI nanofibers of similar sizes to the pure **PANI-F**, and the PANI fibers distribute both on the surface and between the **GO** sheets. This morphology remains in the reduced forms **PAG10** and **PAG50**, indicating that the reduction, reoxidation, and reprotonation process do not have a significant effect on the morphology of the composites. For the composites **PAGO80** and **PAG80** with a less amount of the PANIs component, the fibrous PANIs mainly adsorb on the surface or intercalate between the GO or graphene sheets. The morphology of **PAG80** is very different from the pure **GR**, i.e., the graphene sheets in the **PAG80** mainly exist in wrinkled form with PANI fibers distributed between or on the graphene sheets, while in the pure **GR**, the graphene sheets agglomerate into particles. Such morphology is supposed to stabilize the three-dimensional bulky structure of the composites during the charge−discharge process, which may lead to higher capacitance and longer cycling life. A comparison of the SAED patterns of **PAG10**, **PAG50**, and **PAG80** discloses that with the increase of graphene ratios, the composites also show an increasing of crystalline character, indicating that higher conductivity could be obtained in the composites with higher graphene loadings.

The structure of the composites was also investigated by powder X-ray diffraction (XRD) measurements. The XRD patterns of **PANI-F**, **GO**, **GR**, and all composites are shown in Figure 3. **GO** exhibits a broad reflection with peak at $2\theta = 13.1°$, which is correlated to an interlayer spacing of 0.68 nm in the layer-like **GO**. This value can be

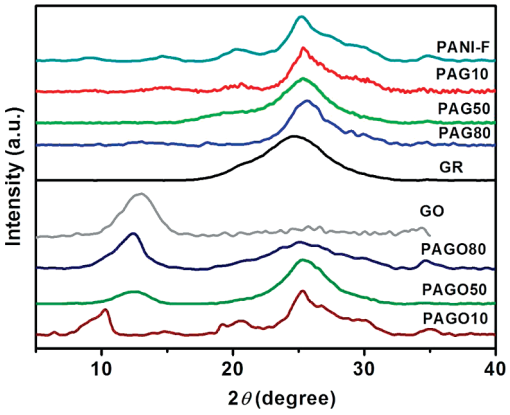

Figure 3. X-ray diffraction patterns of **PANI-F**, **GO**, **GR**, **PAGO10**, **PAGO50**, **PAGO80**, **PAG10**, **PAG50**, and **PAG80**.

assigned to the (001) reflection peak and might depend on the method of preparation and on the number of layers of water in the gallery space of the material.[25] After reduction into pure graphene, one broad reflection peak centered at $2\theta = 24.6°$ was observed in the XRD pattern of **GR**, which can be correlated to an interlayer spacing of 0.36 nm in the graphene sample. The observed broad peak also indicates that the graphene sheets are loosely stacked in **GR**, and it is different from the crystalline graphite. The pure **PANI-F** sample exhibits several broad reflection peaks, with the most intense peak at $2\theta = 25.2°$ (i.e., $d = 0.35$ nm). These reflections indicate some crystalline order in the bulk **PANI-F** samples. Upon intercalation with PANI fibers, the (001) diffraction peaks assigned to the interlayer distance between the GO sheets gradually shift to a smaller angle region (i.e., larger distance) with the increasing of the PANI loading following the sequence of **GO** (0.68 nm), **PAGO80** (0.72 nm), **PAGO50** (0.72 nm), and **PAGO10** (0.85 nm). Such an expansion of layer distance can be explained by the adsorption and intercalation of the PANI fibers on the surface and between the GO sheets as observed in the SEM and TEM images. Along with the interlayer space expansion, the reflection peaks related to the PANI fibers also gradually appear with the increase of the PANI/GO ratios. After reduction, reoxidation, and reprotonation, the typical peaks correlated to the interlayer spacing of graphene oxide completely disappear in all graphene/PANI nanofiber composites, indicating a nearly complete reduction of all GO into graphene sheets. The new peaks correlated to the interlayer space between the graphene sheets however overlap with the diffractions from the PANI nanofibers, and usually broad intense peaks around $2\theta = 25°$ together some weak reflections are observed for **PAG10**, **PAG50**, and **PAG80**.

In order to differentiate the structure of PANI nanofibers in the composite, high-resolution solid-state ^{13}C NMR spectra (Figure S1) and FT-IR spectra (Figure S2) of **PANI-F**, **GO**, **GR**, **PAGO10**, and **PAG10** were collected and shown in the Supporting Information. The solid-state ^{13}C NMR spectrum of **PANI-F** shows a broad peak around 120 ppm. The **GO** exhibits typical resonances at 68, 158, and 220 ppm, which are ascribed to the epoxide, alcohol, lactol, and ketones groups, and the intense peak at 123 ppm is assigned to the graphitic carbons in the **GO**.[26] The ^{13}C NMR spectrum of **GR** after reduction of **GO** by hydrazine only shows a broad upfield-shifted resonance with the peak at about 110 ppm. Resonances from oxygen-containing groups in the **GO** component can also be observed in the solid-state ^{13}C NMR spectrum of **PAGO10**. However, the solid-state ^{13}C NMR spectrum of **PAG10** has a broad peak at about 120 ppm with signals of **PANI-F** and **GR** overlapped together, indicating that the composite is indeed contain the reduced graphene and the polyaniline in the EB form. In the FT-IR spectra, typical peaks of the C=O group at 1732 cm^{-1} were observed from **GO** and **PAGO10**. After reduced by hydrazine, this peak disappeared in the FT-IR spectra of **GR** and **PAG10**, suggesting a complete reduction of the graphene oxide, and this is in agreement with the XRD and solid-state NMR data. The intense peaks at 1577 and 1135 cm^{-1} in **PAGO10** and 1569 and 1135 cm^{-1} in **PANI-F** can be correlated to the quinoidal structure of PANI, and they are much higher than the peaks around 1487 cm^{-1} in **PANI-F** and 1476 cm^{-1} in **PAGO10** which are ascribed to the benzenoid structure of PANI.[24c] After reduction, reoxidation, and reprotonation, **PAG10** exhibits an intense peak at 1497 cm^{-1} (benzenoid rings) together with less intense peaks at 1591 and 1161 cm^{-1} (quinoidal rings), indicating a lower doping level of PANI than that in **PAGO10**.[24c]

The composition and structure of the **PANI-F**, **GO**, **GR**, and the composites were further studied by thermogravimetric analysis (TGA). As shown in Figure 4, all the materials show a little mass loss around 100 °C due to the deintercalation of H_2O. **GO** shows a dramatic mass loss from around 200 to 300 °C due to the decomposition of oxygen-containing groups.[27] After reduction by hydrazine, the obtained graphene sample **GR** only shows 23% mass loss from 100 to 600 °C, indicating that most of the oxygen-containing groups were removed during the chemical reduction process. At the same time, the **PANI-F** sample displays a 40% mass loss from 100 to 600 °C. Compared with **GO**, a mass loss of 30% can be observed for **PAGO80** from 100 to 300 °C. A mass loss of 25% between 100 and 600 °C was observed from sample **PAG80**, similar to the **GR** sample. The relatively larger mass loss of **PAG80** than the pure **GR** after 300 °C should be contributed to the decomposition of the PANI component in the composites. Similar TGA features were observed for the other composites, and usually the composites with graphene component show better thermal

(25) Liu, Z. H.; Wang, Z. M.; Yang, X.; Ooi, K. *Langmuir* **2002**, *18*, 4926.

(26) Gao, W.; Alemany, L. B.; Ci, L.; Ajayan, P. M. *Nat. Chem.* **2009**, *1*, 403–208.

(27) McAllister, M. J.; Li, J.-L.; Adamson, D. H.; Schniepp, H. C.; Abdala, A. A.; Liu, J.; Herrera-Alonso, M.; Milius, D. L.; Car, R.; Prud'homme, R. K.; Aksay, I. A. *Chem. Mater.* **2007**, *19*, 4396–4404.

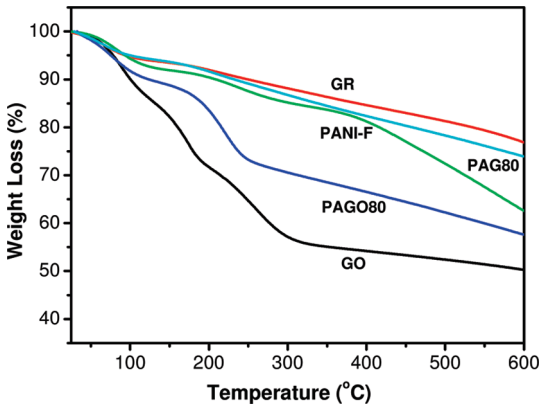

Figure 4. TGA curves of **GO**, **GR**, **PANI-F**, **PAGO80**, and **PAG80** (heating rate = 10 °C/min under a nitrogen atmosphere).

Table 1. List of the Conductivities of All Composites and the Specific Capacitances (F/g) of the Composites at Different Current Loadings Based on Discharge Branch in 2 M H_2SO_4

		cycle 1st			cycle 5th		
samples	conductivity (S/m)	0.1 A/g	0.5 A/g	1 A/g	0.1 A/g	0.5 A/g	1 A/g
PANI-F	10.6	420	145	140	280	140	130
PAGO10	231.3	320	256	199	225	219	170
PAGO50	15.5	207	147	130	195	147	130
PAGO80	0.4	158	148	143	165	148	143
GO	0.2	0.8	-	-	0.8	-	-
PAG10	168.7	214	284	168	212	213	179
PAG50	22.8	180	175	135	155	154	128
PAG80	143.0	480	260	210	410	260	200
GR	277.2	20	-	-	20	-	-

stability with less mass loss compared with the respective **GO**-based composites.

3.3. Electrical Conductivity and Electronic Structure of the Composites. The electrical conductivities (σ) of the **PANI-F**, **GO**, **GR**, and all composite materials were determined on pressed pellets from powder by using an Alessi four-probe resistivity measurement system, and the average conductivities are collected in Table 1. The **GO** sample has a low conductivity of 0.2 S/m similar to that reported in the literature.[14] The **PANI-F** sample is conducting with the conductivity of 10.6 S/m. The **GR** exhibits a much higher conductivity of 277.2 S/m which is close to that of pristine graphite.[17a] As discussed above, the composites prepared by the in situ polymerization have a graphene-like layered structure with PANI nanofibers intercalated between the layers or adsorbed on the surface of the **GO** or **GR** sheets. The homogeneously distributed PANI fibers among **GO** or **GR** sheets would affect greatly on the electrical properties of the composites. The conductivity of **PAGO10** is enhanced dramatically to 231.2 S/m compared with the pure **PANI-F** sample. The conductivity of **PAG10** (σ = 168.7 S/m) decreases a little bit in comparison to the **PAGO10** probably due to the decrease of the doping degree of PANI and the morphology change of the composites during the reduction, reoxidation, and reprotonation processes. Nevertheless, the electrical conductivities of both composites are much higher than that of the pure **PANI-F** sample. Such enhancement of the

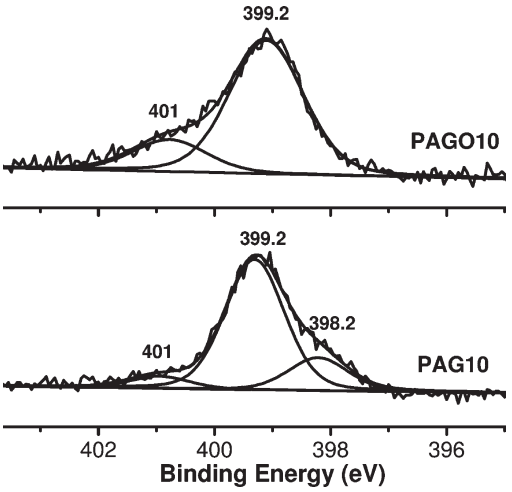

Figure 5. N 1s core-level X-ray photoelectron spectroscopy (XPS) of composites **PAGO10** and **PAG10**.

conductivity might be attributed to the $\pi-\pi$ stacking between the PANI polymer backbone and the **GO** or **GR** sheets. With further increasing of the weight percentage of graphene oxide in the composites, the conductivities decrease due to the insulating effect of **GO**, for example, the **PAGO50** and **PAGO80** show conductivities of 17.5 and 0.4 S/m, respectively. After reduction, reoxidation, and reprotonation, the conductivities of **PAG50** (σ = 22.8 S/m) and **PAG80** (σ = 143.0 S/m) increase due to the recovery of graphene-like structure.

To further understand the different conductivities observed in different composites, X-ray photoelectron spectroscopy (XPS) was used to probe the different electronic structures of the PANI in **PAGO10** and **PAG10**. As shown in Figure 5, the deconvolution of N 1s core-level spectra results in three peaks correlated to three different electronic states: the benzenoid amine with binding energy (BE) centered at 399.4 eV, the quinoid amine with BE at 398.2 eV, and the nitrogen cationic radical (N^+) with BE at 401 eV.[28] It was found that the PANI in the **PAGO10** has typical electronic structures of benzenoid amine and nitrogen cationic radical, but the reoxidized and reprotonated PANI in the **PAG10** presents all three types of amine structures with a decreased percentage of the nitrogen cationic radical and appearance of new quinoid amine structure. These data also indicate a relatively lower doping level of PANI in the **PAG10** than that in the as-formed PANI after in situ polymerization. Such a difference may be due to the slow diffusion of oxidant and acid to the reduced PANI during the reoxidation and reprotonation process. Anyway, the conductivities of these composites after reoxidation and reprotonation still stand at a high level which is essential for their electrical applications such as for supercapacitor electrodes.

3.4. Supercapacitor Characterizations. The potential of using these composites as electrode materials for supercapacitors was tested by standard cyclic voltammetry

(28) Han, M. G.; Cho, S. K.; Oh, S. G.; Im, S. S. *Synth. Met.* **2002**, *126*, 53–60.

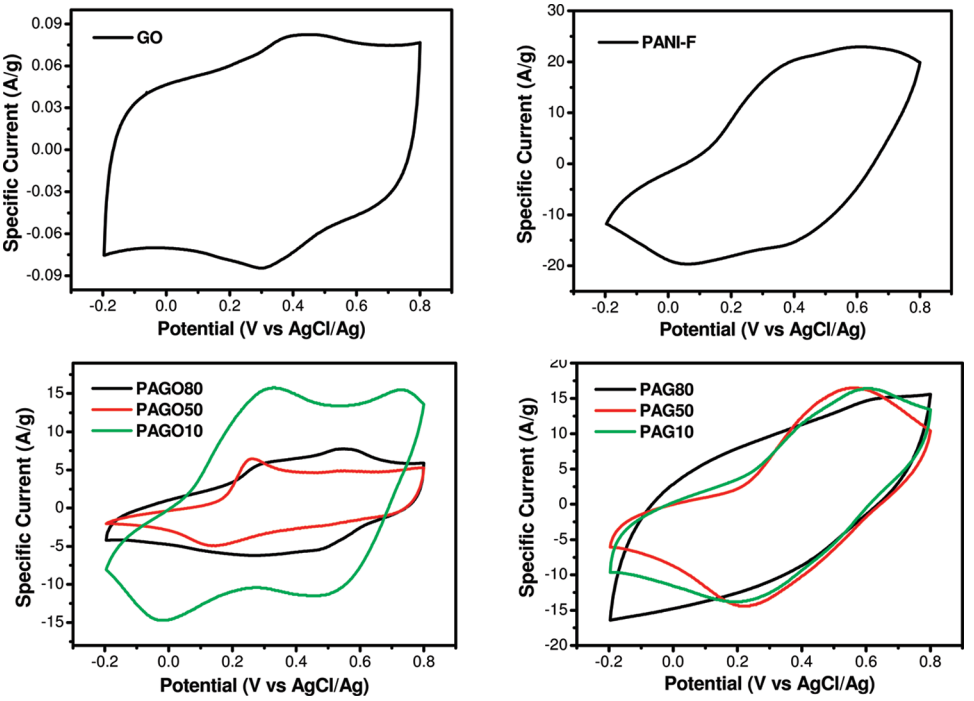

Figure 6. Cyclic voltammograms recorded in 2 M H_2SO_4 by using different composites coated glassy carbon electrode as working electrode, a Pt sheet as counter electrode, and a AgCl/Ag electrode as reference electrode. The scan rate is 100 mV/s.

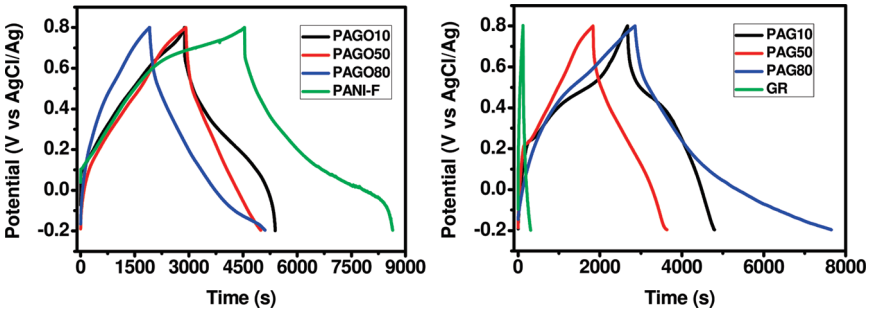

Figure 7. Charge/discharge cycling curves of different composite electrodes at a current density of 0.1 A/g.

(CV) and galvanostatic charge−discharge technique. The potential of using these composites as electrode materials for supercapacitors was tested by standard cyclic voltammetry (CV) and galvanostatic charge−discharge technique. All electrochemistry measurements were conducted in a three-electrode cell, and the working electrode was prepared by casting a nafion-impregnated composite sample onto a glassy electrode. A platinum sheet was used as the counter electrode, and a AgCl/Ag electrode was used as the reference electrode. The electrolyte used is a 2 M H_2SO_4 aqueous solution.

The cyclic voltammograms of the different composite electrodes with a potential window from −0.2 to 0.8 V (vs AgCl/Ag) are shown in Figure 6, and the representative charge/discharge curves at a current density of 0.1 A/g are shown in Figure 7. The average specific capacitance values, C_{avg} (F/g) of the samples were estimated from the discharge process according to the following equation

$$Cg = \frac{I\Delta t}{\Delta V \times m} \quad (1)$$

where I is the current loaded (A), Δt is the discharge time (s), ΔV is the potential change during discharge process, and m is the mass of active material in a single electrode (g). All specific capacitance data under the first and fifth cycle with different current loadings are collected in Table 1.

It can be seen that the CV curve of **GO** shows only one pair of redox peaks due to the transition between quinone/hydroquinone states, which is typical for carbon materials with oxygen-containing functionalities.[29] The CV curve is nearly rectangular in shape, indicating good charge propagation within the electrode. However, the specific capacitance is less than 1 F/g probably due to the low conductivity. Two couples of redox peaks are observed from the CV curve of **PANI-F**, corresponding to redox transitions of leucoemeraldine form (semiconductor)/polaronic emeraldine form (conductor) and Faradic transformation of emeraldine/pernigraniline.[30] Similar to the reported values for the PANI based

(29) Nian, Y. R.; Teng, H. S. *J. Electrochem. Soc.* **2002**, *149*, A1008–A1014.
(30) Wang, Y. G.; Li, H. Q.; Xia, Y. Y. *Adv. Mater.* **2006**, *18*, 2619–2623.

supercapacitors, high specific capacitance of 420 F/g is obtained for the fibrous **PANI-F** sample. However, typical poor stability of the specific capacitance during cycling is also observed (Table 1).[7] It decreases significantly with the increment of scan current density, from 420 F/g at 0.1 A/g to 140 F/g at 1 A/g as well as with increasing of the cycle numbers, from 420 F/g at the first cycle to 280 F/g at the fifth cycle. During the doping/dedoping process, the PANI electrode undergoes swelling, shrinkage, cracking, or breaking that induces gradually deterioration of the conductivity and volumetric changes.[31]

As described by various characterizations above, PANI fibers intercalated into the **GO** or **GR** sheets interlayer space generates the hybrid materials in which two types of low dimensional electrical conductors coexist homogenously at a nanometer level. Thus, the PANI-intercalated **GO** composites such as **PAGO10**, **PAGO50**, and **PAGO80** show typically two pairs of redox peaks (Figure 6). The features for PANI in their CV curves decrease with the decreasing of the PANI weight percent in the composites. The specific capacitances of these hybrid materials increase, while the PANI/**GO** ratio in composites increased, from **PAGO80** (158 F/g), to **PAGO50** (207 F/g), to **PAGO10** (320 F/g). However, all the specific capacitances of these **GO** containing composites are still lower than that of pure **PANI-F**. This suggests that the insulating **GO** sheets in the composites contribute little to the specific capacitance, and the total capacitance is mainly dominated by the pseudocapacitance from the conducting PANI nanofibers. However, as shown in Table 1, the cycling stability of **PAGO80** and **PAGO50**, with less than a 5% decrease at various current densities from the first cycle to the fifth cycle, is much better than that of **PAGO10**, which shows a 10−30% loss from the first cycle to the fifth cycle. These data suggest that introduction of **GO** sheets can significantly improve the cycling stability of supercapacitors likely due to the homogeneous dispersion of **GO** sheets among the PANI matrix.

After reduction, reoxidation, and reprotonation, the CV curves of all graphene/PANI composites become more featureless (Figure 6). This may be accounted for the removal of oxygen-containing groups from the **GO** sheets and the change of the PANI structure during these processes. The specific capacitances of **PAG10** and **PAG50** are 214 F/g and 180 F/g, respectively, at a current density of 0.1 A/g (Table 1). The decreased specific capacitances compared with those of **PAGO10** and **PAGO50** could be ascribed to the changed electronic structure and morphology of the PANI in the composites. However, the highest specific capacitance of 480 F/g at 0.1 A/g is obtained from the capacitors based on **PAG80**. Meanwhile, **PAG80** also shows better cycling stability than other composites, with the first cycle specific capacitance of 480 F/g and the fifth cycle specific capacitance of 410 F/g at 0.1 A/g. In addition, when the current density is increased up to 0.5 A/g and even 1 A/g, the specific capacitances still remain at a high level above 200 F/g without a significant decrease upon the charge−discharge cycling. The cycling electrochemical stability of the electrode based on composite **PAG80** was examined by charge−discharge cycling at the current density of 1.5 A/g, and the result are shown in Figure S3. It was seen that over 70% of the original capacitance was retained after 400 cycles and lasted over 1000 cycles, showing this electrode material had a good cycling stability.

Impedance measurements were performed for **GO**, **GR**, **PANI-F**, and all the composites in 2 M H_2SO_4 aqueous electrolyte by the electrochemical impedance spectroscopy (EIS). EIS is a technique complementary to galvanostatic cycling measurements which provides more information on the electrochemical frequency behavior of the system. Impedance measurements can also study the redox reaction resistance and equivalent series resistance. EIS were collected with a frequency range of 0.1 Hz-10 kHz and a DC bias of 10 V.

The EIS data were analyzed using Nyquist plots. Nyquist plots show the frequency response of the electrode/electrolyte system and are a plot of the imaginary component (Z") of the impedance against the real component (Z'). Each data point is at a different frequency with the lower left portion of the curve corresponding to the higher frequencies. The more vertical the curve corresponds to a cell more closing to an ideal capacitor. As shown in Figure 8, the equivalent series resistance (ESR) of the electrode can be obtained from the x intercept of the Nyquist plot. All the materials show comparable ESR at about 2 Ω. The Nyquist plots of **GO**, **PANI-F**, **PAGO10**, **PAGO50**, **PAGO80**, **PAG10**, and **PAG50** exhibit a semicircle over the high frequency range, followed by a straight 45° sloped line in the low frequency region. Large semicircles observed for these electrodes are indicative of high interfacial charge-transfer resistance, which can be attributed to the poor electrical conductivity of these materials. The 45° sloped portion of the Nyquist plots is the Warburg resistance resulting from the frequency dependence of ion diffusion/transport in the electrolyte. The larger Warburg region of these electrodes indicate greater variations in ion diffusion path lengths and increased obstruction of ion movement. Different from **GO**, the semicircle at high frequency is not detected for **GR**, suggesting that interfacial charge-transfer resistance among **GR** is significantly low, because of the high conductivity. Similar to **GR**, **PAG80** has neglectable interfacial charge-transfer resistance apparently, which can be attributed to the low content of PANI nanofibers and the high conductivity of **GR** sheets. Except for the low electrical resistance, **PAG80** also exhibits short and equal diffusion path length of the ions in the electrolyte, which can be seen from the neglectable Warburg region on the Nyquist plots. This may be illuminated by the unique morphology of this composite. A small amount of PANI nanofibers in **PAG80** are distributed homogeneously on

(31) (a) Khomenko, V.; Frackowiak, E.; Béguin, F. *Electrochim. Acta* **2005**, *50*, 2499–2506. (b) Li, L.; Song, H.; Zhang, Q.; Yao, J.; Chen, X. *J. Power Sources* **2009**, *187*, 268–274.

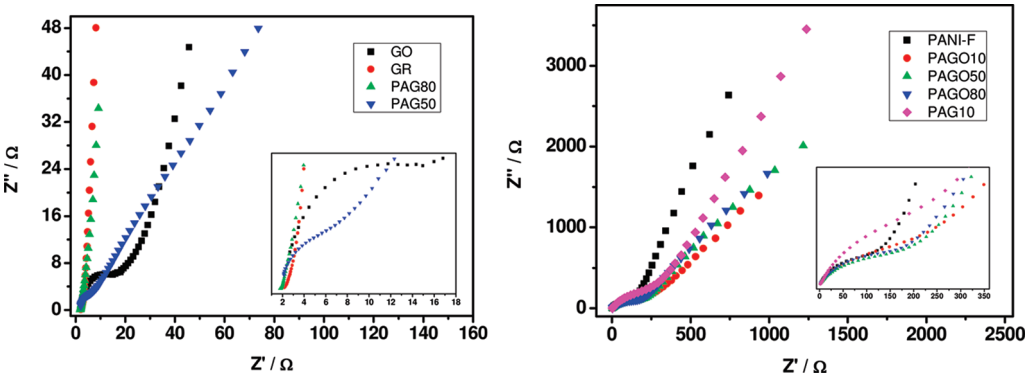

Figure 8. Nyquist plots of different composites electrodes.

the surface of layered graphene sheets. Thus, the ions of electrolyte do not penetrate into the particulate and access only the surface of PANI nanofibers.

The specific capacitance of the **PAG80** composite is higher than that of graphene,[17a,c] carbon nanotube,[12] carbide-derived carbon,[5] and activated carbon.[5] The specific capacitance of the **GR** sample is only about 20 F/g at a current density of 0.1 A/g. Such a low EDL capacitance may be ascribed to its low BET surface area at only 7.9 m^2/g. Considering the similar low BET surface areas of all the composites, i.e. 4.3−20.2 m^2/g (see Table S1 in the Supporting Information), the much higher specific capacitance of **PAG80** compared with that of **GR** should be mainly ascribed to the pseudocapacitance from the PANI nanofibers in the composite. Moreover, it should be noted that both the specific capacitance and the stability of the electrode based on **PAG80** are much better than those of the electrode based on **PANI-F**. Thus we can say dispersing PANI nanofibers into a carbonaceous matrix with high conductivity, like **GR**, could largely improve its specific capacitance and cycling stability. Meanwhile, such **GR** or **GO** doped PANI composites are also supposed to enhance the mechanical strength of the composite materials, and a further study is under investigation.

4. Conclusions

In summary, a series of homogeneous composites of chemically modified graphene and polyaniline is prepared by in situ polymerization. Meanwhile, the mass ratios of chemically modified graphene and polyaniline are tuned to make the composites with polyaniline as the main component (**PAGO10**/**PAG10**) or with chemically modified graphene as the main component (**PAGO80**/**PAG80**) or with a roughly equal ratio in the blend (**PAGO50**/**PAG50**). The morphology and structure of these composites and the pure polyaniline fibers (**PANI-F**), graphene oxide (**GO**), and graphene (**GR**) are fully characterized by different techniques such as XRD, IR, solid-state ^{13}C NMR, SEM, TEM, TGA, and XPS. It is clear that PANI nanofibers and the chemically modified graphene form a homogeneous composite at the nanometer scale with the PANI fibers distributed on the surface or between the graphene/GO sheets. Most of the composites show high electrical conductivities which are essential for their applications as electrode materials for supercapacitors. High specific capacitances and good cycling stability are achieved for most composites with the highest specific capacitance of 480 F/g at a current density of 0.1 A/g for **PAG80**. Our results prove that high specific capacitance and good cycling stability can be obtained either by doping the carbon materials with a small amount of PANI or by doping bulky PANI with a small amount of carbon materials due to the significant change of the composite structure. Further tuning and control of the component structure (e.g., by using other conducting polymers), composite ratios, and composite microstructures to exploit better graphene-based electrode materials are undergoing in our lab.

Acknowledgment. This work was financially supported by A*Star SERC Thematic Strategic Research Programme - Sustainable Materials: Composites & Lightweights (R-143-000-401-305), NRF Competitive Research Program (R-143-000-360-281), and Ministry of Education (MOE2008-T2-1-004). We gratefully thank Dr. Gopinadhan Kalon for his kind assistance on the conductivity measurements.

Supporting Information Available: Figures S1−S4 and Table S1. This material is available free of charge via the Internet at http://pubs.acs.org.